Temperature modulation of the optical transitions involving the Fermi surface in Ag: Theory

R. Rosei
Istituto di Fisica, Università di Roma, Roma, Italy
and Gruppo Nazionale di Struttura della Materia of the Consiglio Nazionale delle Ricerche, Roma, Italy
(Received 16 August 1973)

The thermomodulation mechanism for optical transitions originating or terminating near the Fermi surface in noble metals has been investigated. Detailed thermoderivative line shapes of $\Delta\epsilon_2$ for both inter-conduction-band transitions and transitions from the d bands to the Fermi surface have been calculated for Ag. The calculation also gives the temperature dependence of the joint density of states for these transitions.

I. INTRODUCTION

In the last few years, much effort has been devoted to a deeper understanding of the electronic structure of the noble metals.[1-8] Refined theoretical methods are now available for more reliable band-structure calculations,[8-10] and photoemission[11-17] and optical[18-28] measurements (both of the static and derivative or modulated type) have provided very detailed information on the electronic structure many eV away from the Fermi surface.

It is fairly well established that the strong interband edge in Ag at about 3.9 eV is of a composite nature,[5,6] the strong $L_3 \rightarrow L_2'(E_F)$ transitions (d band to Fermi surface near L) being overlapped by weaker transitions near $L_2'(E_F) \rightarrow L_1$. Both optical[19,20,23,29,30] and photoemission[11,17,31,32] results support this interpretation which, however, has been questioned recently by Christensen.[10,33]

Several questions [such as the exact position of the onset of the $L_2'(E_F) \rightarrow L_1$ transition as well as the position of the $L_2' \rightarrow L_1$ critical point[34]] are still open. Another aspect of theoretical interest is the exact determination of the ratio of the oscillator strengths of the two overlapping transitions.

Recent work on thermomodulation at very low temperature on Au[35] has proved very useful for untangling d-band–to–Fermi-surface optical transitions from the large number of signal sources in derivative experiments on noble metals. It also provided the first attempt at giving a quantitative account of the modulation mechanism for transitions of this kind.

In the following a more comprehensive account of this modulation mechanism is given, and the calculation has been extended to inter-conduction-band transitions involving the Fermi surface. Experimental results of thermomodulation measurements taken at very low temperature on Ag are reported in the following paper[36] (referred to henceforth as paper II) and interpreted in the light of the theory presented below.

II. INTER-CONDUCTION-BAND TRANSITIONS [$L_2'(E_F) \rightarrow L_1$]

A. Static joint density of states

The inter-conduction-band transitions occurring

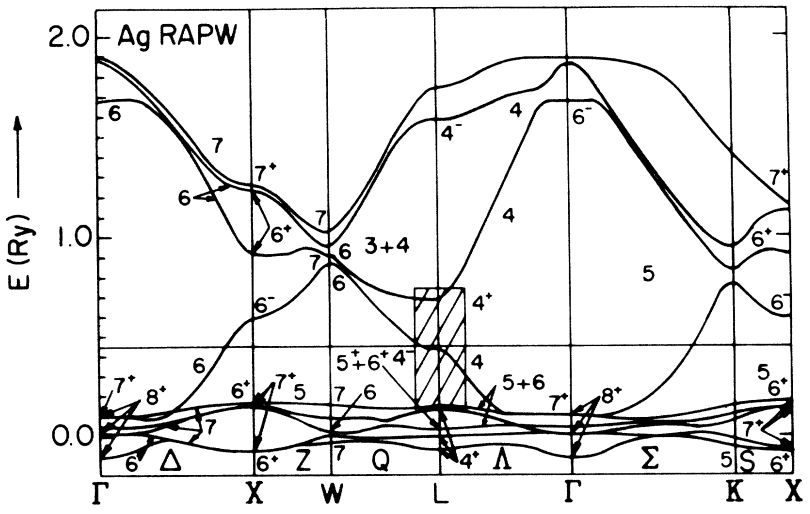

FIG. 1. Relativistic band structure of Ag as calculated by Christensen (Ref. 10). The hatched area is of particular interest for optical interband absorption.

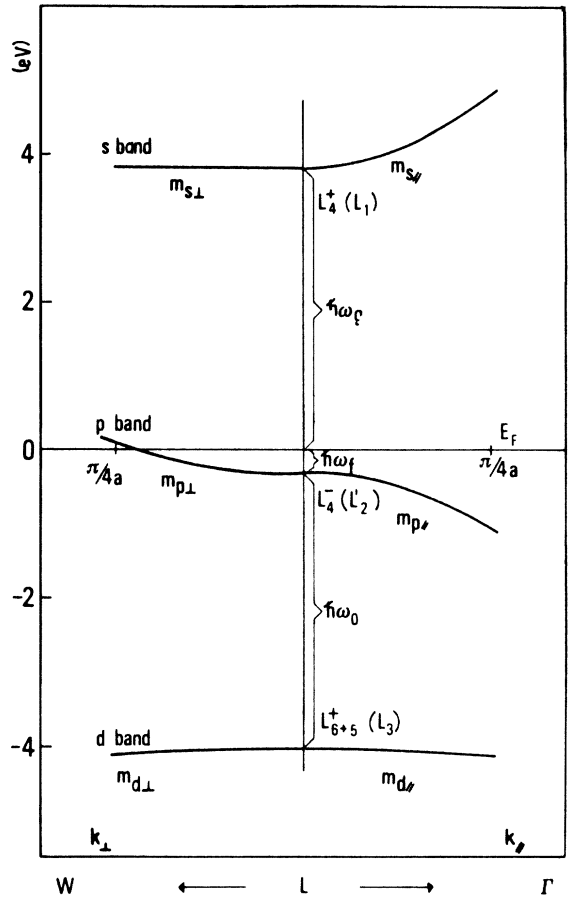

FIG. 2. Detail of the band structure near L for Ag.

near L in Ag are strongly influenced by the existence of the Fermi surface. Figure 1 shows the relativistic augmented-plane-wave band structure calculated by Christensen.[10] The hatched area is of particular interest in optical experiments because most of the optical interband absorption involves these bands. Figure 2 shows this region in greater detail.

If the p band were completely occupied, the $p \rightarrow s$ transitions would give an M_2-type critical point in the joint density of states (JDOS). Since the band is filled only up to the Fermi level, we can have optical transitions only for photon energies above a well-defined threshold $\hbar\omega_1$, which is shown in Fig. 3(a). The shape for the JDOS which we expect is shown schematically in Fig. 3(b).

Assuming the energy bands depend quadratically on the distance from L, the shapes of the JDOS $(\hbar\omega, T)$ and the related optical function $\epsilon_2(\hbar\omega, T)$ can be calculated in closed form. From the latter, the derivative $\partial\epsilon_2/\partial T$ can be calculated, allowing a meaningful comparison with thermoderivative experimental data. Referring to Fig. 2 and assuming rotational symmetry around the direction L-Γ, we may write for the p and s bands[37]

$$\hbar\omega_p = -\hbar\omega_f + \frac{\hbar^2}{2m_{p\perp}} k_\perp^2 - \frac{\hbar^2}{2m_{p\parallel}} k_\parallel^2 \ , \tag{1}$$

$$\hbar\omega_s = \hbar\omega_g + \frac{\hbar^2}{2m_{s\perp}} k_\perp^2 + \frac{\hbar^2}{2m_{s\parallel}} k_\parallel^2 \ , \tag{2}$$

where $k_\perp$ is defined as

$$k_\perp = (k_x^2 + k_y^2)^{1/2} \ , \tag{3}$$

k_x and k_y being along orthogonal axes in the hexagonal face through L.

Considering only direct or vertical transitions, if $\hbar\omega_s(k)$ and $\hbar\omega_p(k)$ denote energies in the final band s and in the initial band p, respectively, then transitions between these two bands at photon energy $\hbar\omega$ are restricted to the surface of constant interband energy given by

$$\Omega_{sp}(\vec{k}) \equiv \hbar\omega_s(\vec{k}) - \hbar\omega_p(\vec{k}) - \hbar\omega = 0 \ . \tag{4}$$

The JDOS for the bands we are considering is defined as[31,38]

$$\mathcal{J}_{p\rightarrow s}(\hbar\omega) = \frac{1}{(2\pi)^3} \int' d^3k\, \delta(\Omega_{sp}(\vec{k})) \ . \tag{5}$$

The prime on the integral denotes that the integration is to be performed only over those portions of k space for which $\hbar\omega_s > E_F > \hbar\omega_p$.

As is well known,[39] it is possible to integrate

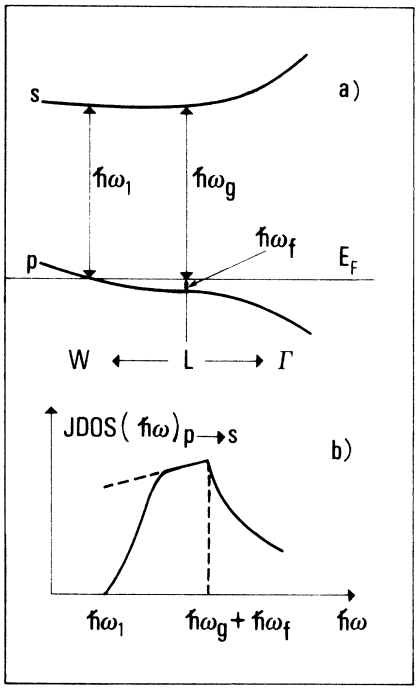

FIG. 3. (a) Bands responsible for inter-conduction-band transitions in Ag. (b) Schematic joint density of states for the $p \rightarrow s$ transitions in Ag (solid line).

over the δ function in Eq. (5). The JDOS reduces then to the form

$$\mathcal{J}_{p\to s}(\hbar\omega) = \frac{1}{(2\pi)^3}\int' \frac{dS_{sp}}{|\nabla_{\vec{k}}(\hbar\omega_s) - \nabla_{\vec{k}}(\hbar\omega_p)|} \quad , \tag{6}$$

the integral being carried out over the surface $\Omega_{sp}(\vec{k}) = 0$.

The surfaces where the band p has constant initial energy E and the band s has constant final energy $E + \hbar\omega$ are easily written:

$$\hbar\omega_p(\vec{k}) \equiv -\hbar\omega_f + \frac{\hbar^2}{2m_{p\perp}}k_\perp^2 - \frac{\hbar^2}{2m_{p\parallel}}k_\parallel^2 = E \quad , \tag{7}$$

$$\hbar\omega_s(k) \equiv \hbar\omega_g + \frac{\hbar^2}{2m_{s\perp}}k_\perp^2 + \frac{\hbar^2}{2m_{s\parallel}}k_\parallel^2 = E + \hbar\omega \quad . \tag{8}$$

The surface $\Omega_{sp}(k) = 0$, usually called CEDS[9] (constant-energy-difference surface), is obtained by subtracting Eq. (7) from Eq. (8):

$$\Omega_{sp}(k) \equiv \hbar\omega_g + \hbar\omega_f + \frac{\hbar^2}{2}\left(\frac{1}{m_{s\perp}} - \frac{1}{m_{p\perp}}\right)k_\perp^2 + \frac{\hbar^2}{2}\left(\frac{1}{m_{s\parallel}} + \frac{1}{m_{p\parallel}}\right)k_\parallel^2 - \hbar\omega = 0 \quad . \tag{9}$$

Figure 4 shows the (110) section of the Fermi surface as calculated from Eq. (7) together with several (110) sections of CEDS's calculated for different photon energies from Eq. (9).[40]

For $\hbar\omega = 3.76$ eV, CEDS IV runs outside the Fermi surface and corresponds to empty states in the p band. Therefore, no transition can occur. When the photon energy is increased, the surface cuts through the Fermi surface and optical absorption starts, increasing with the area of CEDS, which runs inside the Fermi surface. The calculation of the JDOS ($\hbar\omega$) is therefore very easy at

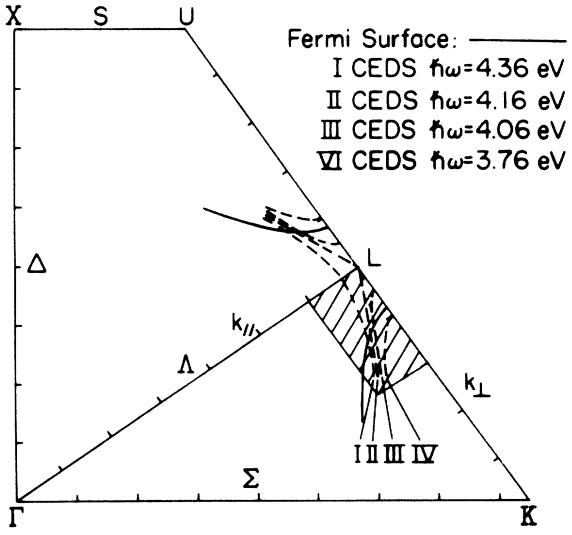

FIG. 4. (110) sections of CEDS and Fermi surface.

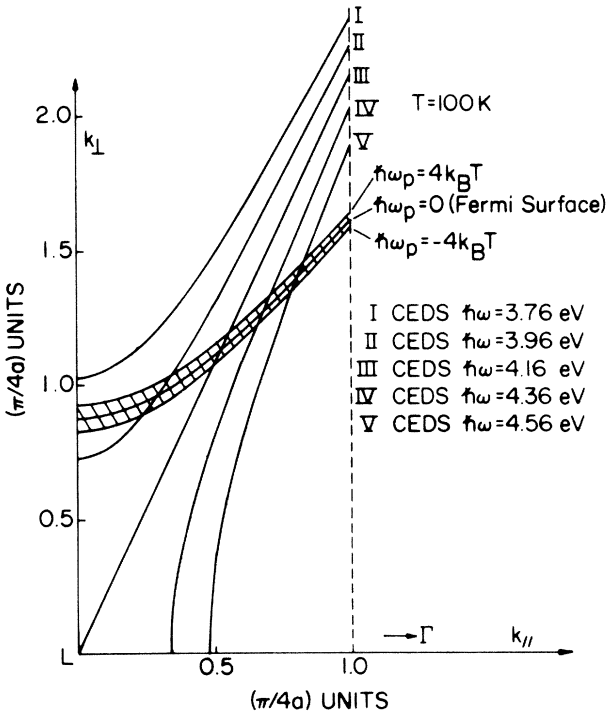

FIG. 5. Cross section in the Fermi-surface neck region of CEDS ($p \to s$ bands) in a plane containing the L-Γ direction. The hatched area between the constant-initial-energy surfaces $E = 4k_BT$ and $E = -4k_BT$ show the region in k space where the occupation probability goes from nearly 1 to nearly 0 ($T = 100$ K).

$T = 0$ when the Fermi surface is perfectly sharp. For a finite temperature $T \neq 0$ the situation is slightly complicated by the smearing of the Fermi surface. Figure 5 shows a section of the Brillouin Zone near L (corresponding to the hatched area of Fig. 4). Besides the Fermi surface, the surfaces of constant initial energy $E = 4k_BT$ and $E = -4k_BT$ (for $T = 100$ K) have been plotted. The hatched area between these two surfaces represent the volume in k space where the occupation probability decreases from nearly 1 to nearly 0 when $T = 100$ K.

In calculating the JDOS each infinitesimal ribbon of a CEDS corresponding to transitions with initial energy between E and $E + dE$ has to be weighted with the probability $f(E)$ that the initial state is occupied.

To perform this calculation we borrow from photoemission theory the concept of energy distribution of the joint density of states (EDJDOS). This is formally defined by

$$\mathcal{D}_{p\to s}(E, \hbar\omega) = (2\pi)^{-3}\int d^3k\,\delta(\Omega_{sp}(\vec{k}))\,\delta(E - \hbar\omega_p(\vec{k})) \quad . \tag{10}$$

As discussed, for example, by Koyama and Smith,[41] the extra δ function picks out those transitions

whose initial states lie at energy E. The expression for the EDJDOS may be converted to a line integral[42]:

$$\mathfrak{D}_{p\to s}(E,\hbar\omega)=(2\pi)^{-3}\int\frac{dl_{sp}}{|\nabla_{\vec{k}}(\hbar\omega_s)\times\nabla_{\vec{k}}(\hbar\omega_p)|}\ . \quad (11)$$

The integral is performed around the line of intersection of the two constant-energy surfaces $\hbar\omega_p=E$ and $\hbar\omega_s=E+\hbar\omega$.

Owing to the rotational symmetry around Λ the calculation of the integral is straightforward. The paths of integration turn out to be circles on planes perpendicular to Λ and centered on the Λ axis.[17] Inserting Eqs. (1) and (2) into Eq. (11) one easily obtains

$$\mathfrak{D}_{p\to s}(E,\hbar\omega)=(16\pi^2\hbar^2)^{-1}\mathfrak{F}_{p\to s}\times\left((E+\hbar\omega-\hbar\omega_g)\frac{\hbar}{m_{p\perp}}-(E+\hbar\omega_f)\frac{\hbar}{m_{s\perp}}\right)^{-1/2}, \quad (12)$$

where the factor $\mathfrak{F}_{p\to s}$ is given by

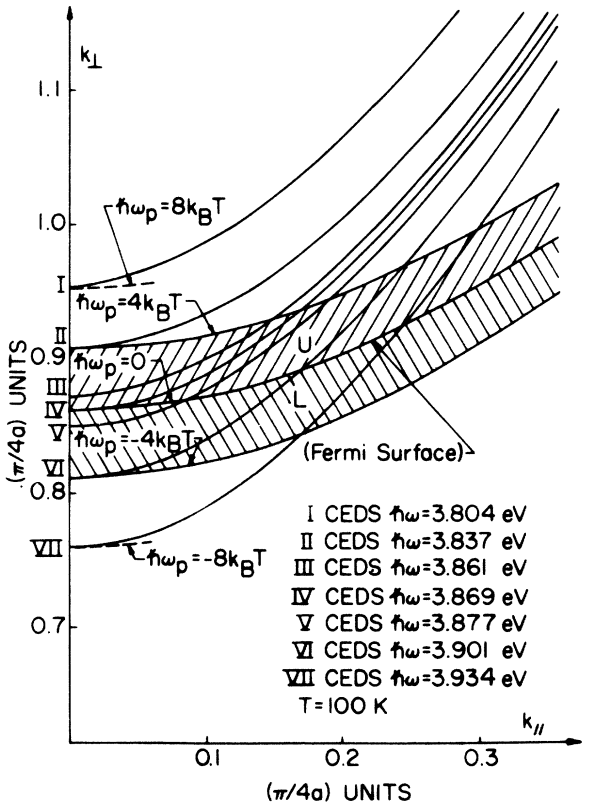

FIG. 6. Detail of the Fermi-surface neck region showing several (110) cross sections of CEDS's ($p\to s$ bands) and constant-initial-energy surfaces. Region L (lower) experiences a decrease in electron population during a small temperature increase (at $T=100$ K) while region U (upper) experiences an increase.

$$\mathfrak{F}_{p\to s}=\left(\frac{m_{s\parallel}\,m_{p\perp}+m_{s\perp}\,m_{p\parallel}}{m_{s\parallel}\,m_{p\parallel}\,m_{s\perp}\,m_{p\perp}}\right)^{-1/2}\ . \quad (13)$$

The EDJDOS exhibits an inverse-square-root singularity[43] as already found for instance by Lindau *et al.*[17] This singular behavior can be understood easily from Fig. 6, which shows in great detail part of the neck region. Close to the hexagonal face of the Brillouin Zone, each CEDS becomes tangent to a surface of constant initial energy, giving rise to a very large number of states with the same initial energy.

The calculation of the JDOS and its temperature dependence is now straightforward:

$$\mathfrak{J}_{p\to s}(\hbar\omega,T)=\int_{E_{\min}}^{E_{\max}}\mathfrak{D}_{p\to s}(E,\hbar\omega)f(E,T)\,dE\ , \quad (14)$$

$f(E,T)$ being the Fermi distribution function.

In the constant-matrix-element approximation the JDOS is easily related to the imaginary part of the dielectric function[44]:

$$\epsilon_2^{p\to s}(\hbar\omega,T)=\frac{8\pi^2e^2\hbar^4}{3m^2}\frac{|P(s\to p)|^2}{(\hbar\omega)^2}\,\mathfrak{J}_{p\to s}(\hbar\omega,T)\ . \quad (15)$$

We are left with the calculation of the integration limits. The calculation of the lower limit is immediate. One obtains

$$E_{\min}=-\hbar\omega_f+\frac{m_{s\perp}}{m_{s\perp}-m_{p\perp}}[\hbar\omega_g+\hbar\omega_f-\hbar\omega]$$
$$\text{for } \hbar\omega<\hbar\omega_g+\hbar\omega_f \quad (16)$$

and

$$E_{\min}=-\hbar\omega_f-\frac{m_{s\parallel}}{m_{p\parallel}+m_{s\parallel}}[\hbar\omega-(\hbar\omega_f+\hbar\omega_g)]$$
$$\text{for } \hbar\omega>\hbar\omega_f+\hbar\omega_g\ . \quad (17)$$

The upper limit of integration $E_{\max}$ has been chosen at the intersection of each CEDS with a plane perpendicular to Λ at a distance $\pi/4a$ from L (shown in Fig. 5). We obtain

$$E_{\max}=-\hbar\omega_f-\frac{\hbar^2}{2m_{p\parallel}}\left(\frac{\pi}{4a}\right)^2+\frac{m_{s\perp}}{m_{s\perp}-m_{p\perp}}\times\left[\frac{\hbar^2}{2}\left(\frac{1}{m_{s\parallel}}+\frac{1}{m_{p\parallel}}\right)\left(\frac{\pi}{4a}\right)^2+(\hbar\omega_g+\hbar\omega_f-\hbar\omega)\right]\ . \quad (18)$$

This procedure may seem somewhat arbitrary at first sight, but in the energy range of interest the upper cut is actually provided by the Fermi surface. The portions of a CEDS a few k_BT above the Fermi surface already give, in fact, a negligible contribution to the absorption.

Figure 7 shows the JDOS obtained for three different temperatures. The magnitude of the JDOS depends on the geometrical factor $\mathfrak{F}_{p\to s}$ given by Eq. (13) as well as on the matrix element of the transition. The latter has been chosen in order to

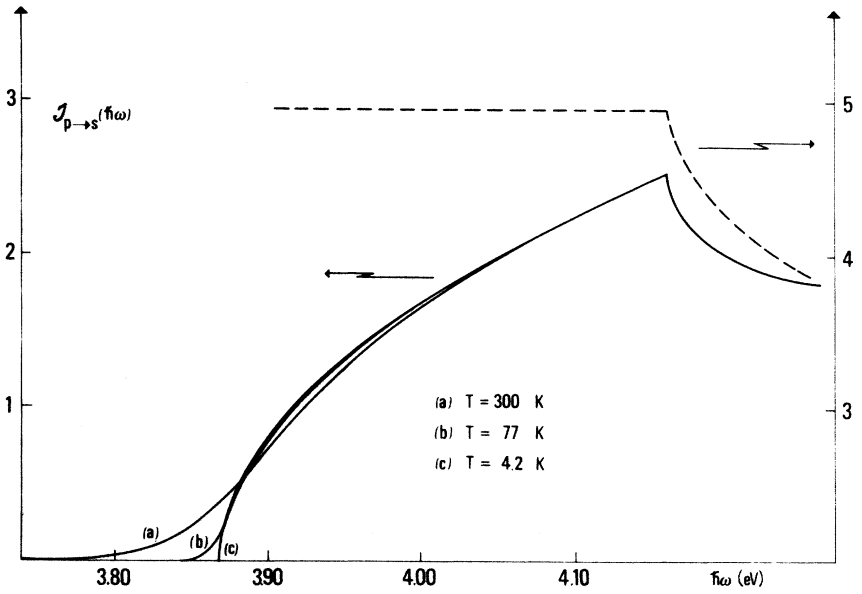

FIG. 7. Joint density of states (JDOS) of Ag due to the inter-conduction-band transitions near L calculated at different temperatures. The dashed line shows the JDOS that would be obtained were the p band completely filled.

obtain agreement with the experimental results presented in paper II. The dashed line in Fig. 7 shows what the JDOS would be were the p band completely occupied: The characteristic shape of an M_2 critical point is clearly seen.

B. Thermoderivative behavior

In a thermoderivative measurement a small temperature wave is applied to a sample and the resultant ac component of the reflectivity and/or transmission is measured. From these data, the change of the imaginary part of the dielectric function ϵ_2 is usually obtained. Many different sources of signal may contribute to thermomodulation spectra in metals[45] but it has been shown[35] that, at sufficiently low temperature, the dominant mechanism is due to the periodic smearing out of the Fermi surface.

The calculation of the JDOS we have been carrying out now allows us to calculate the theoretical $\Delta\epsilon_2$ which should be expected from the inter-conduction-band transitions in a thermomodulation experiment. Differentiating Eq. (14) with respect to T we obtain

$$\Delta\mathcal{J}_{p\to s}(\hbar\omega, T) = \frac{\partial}{\partial T}\mathcal{J}_{p\to s}(\hbar\omega, T)\,\Delta T \quad , \tag{19}$$

where

$$\frac{\partial}{\partial T}\mathcal{J}_{p\to s}(\hbar\omega, T) = \int_{E_{min}}^{E_{max}} \mathfrak{D}_{p\to s}(E, \hbar\omega)\frac{\partial}{\partial T} f(E, T) \tag{20}$$

and ΔT is the amplitude of the temperature modulation. The change of the imaginary part of the dielectric function can be obtained immediately:

$$\Delta\epsilon_2^{p\to s}(\hbar\omega, T) = \frac{8\pi^2 e^2\hbar^4}{3m^2}\,\frac{|P(s\to p)|^2}{(\hbar\omega)^2}\,\Delta\mathcal{J}_{p\to s}(\hbar\omega, T) \quad . \tag{21}$$

Figure 8 shows spectra of $\Delta\epsilon_2^{p\to s}$ obtained at different temperatures, assuming $\Delta T = 1$ K. On lowering the temperature, the structure becomes much sharper and considerable enhancement is ob-

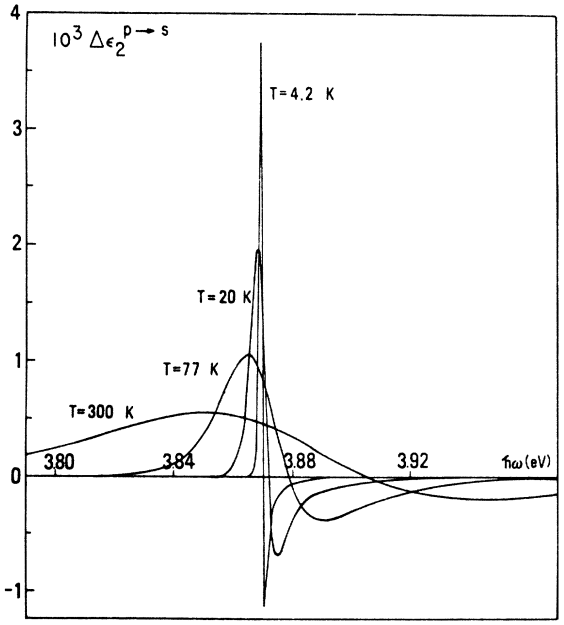

FIG. 8. $\Delta\epsilon_2$ thermomodulation spectra calculated at different temperatures arising from inter-conduction-band transitions in Ag.

tained. At low temperature we may expect good agreement with the experimental $\Delta\epsilon_2$ spectra, but care should be taken when comparing high-temperature spectra with experimental results, which also involve the effect of the other modulation mechanisms.[35,45]

The physical mechanism through which the JDOS is modulated (and with the JDOS, all the optically related functions) can be understood easily. Referring to Fig. 6, the shaded area shows the volume in k space where the thermomodulation phenomena take place at a temperature $T = 100$ K. The spectrum of $\Delta\epsilon_2$ at this temperature is shown in detail in Fig. 9.

On increasing the temperature a small amount the region U (upper) between the Fermi surface and the constant-energy surface $\hbar\omega_p = 4k_BT$ experiences an increase of electron population, while the region L (lower) between the Fermi surface and the constant-energy surface $\hbar\omega_p = -4k_BT$ experiences a decrease. CEDS I at 3.804 eV (which starts $8k_BT$ above the Fermi surface) is too far above this region, so no change whatsoever in absorption at this energy can occur. The arrow (a) in Fig. 9 shows in fact that for this energy $\Delta\epsilon_2$ is zero.

For $\hbar\omega_p = 3.837$ eV CEDS II starts touching the constant-energy surface $\hbar\omega_p = 4k_BT$. Therefore, on increasing the temperature there is a slight increase in electron population which, in turn, gives rise to an increase in absorption [arrow (b) in Fig. 9].

It is interesting also to plot the integrand of Eq.

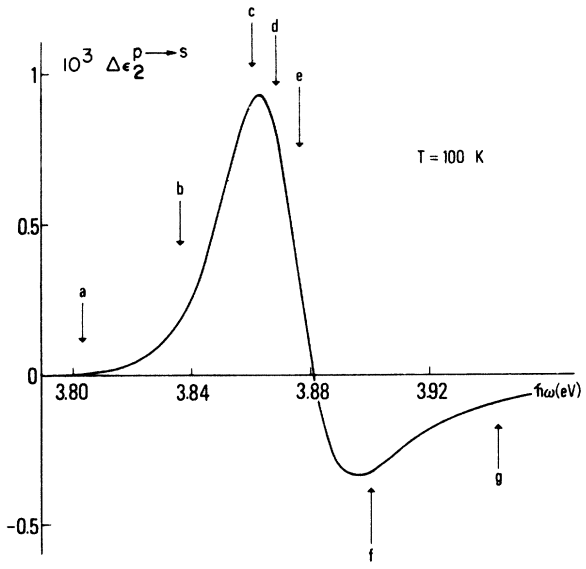

FIG. 9. $\Delta\epsilon_2$ thermomodulation spectrum for interconduction-band transitions in Ag at 100 K. Arrows (a)–(g) indicate the situation corresponding to the CEDS's I–VII, respectively, shown in Fig. 6.

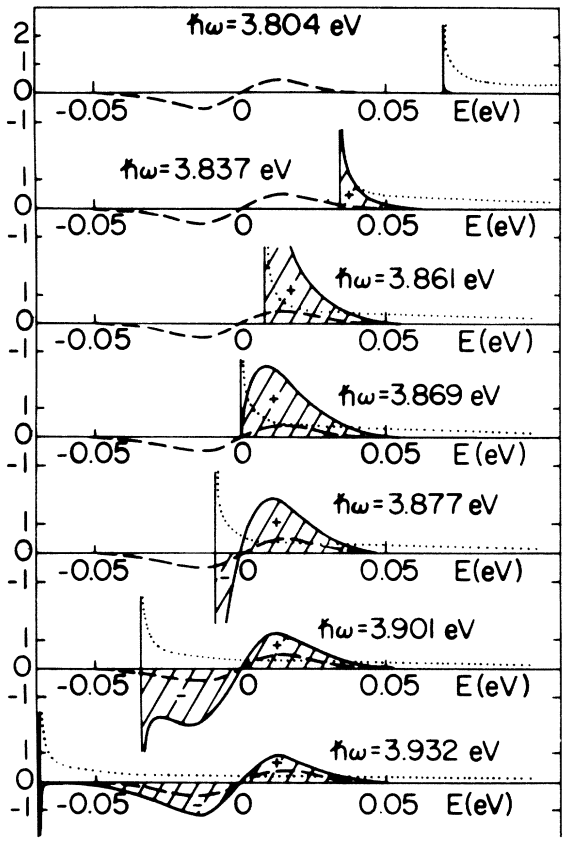

FIG. 10. Thermomodulation mechanism for interconduction-band transitions. The dotted line gives the EDJDOS (E) for several photon energies. The dashed line gives the temperature derivative of the Fermi distribution (at 100 K) and the solid line gives in each case the product E times $\partial f/\partial T$, the integrand of Eq. (20). The algebraic sum of the negative and positive areas (hatched in the figure) gives the net $\Delta\vartheta_{p\to s}(\hbar\omega)$.

(20) separated into its factors (Fig. 10). For each photon energy, the algebraic sum of the negative and positive areas gives the net $\Delta\vartheta_{p\to s}(\hbar\omega)$.

CEDS III has a large part of its surface in region U, therefore giving a large increase of absorption in phase with the temperature wave. CEDS IV should, at first sight, give the maximum positive change in $\Delta\epsilon_2$ since it has more surface than any other CEDS in region U. This is not the case, however [see arrow (d) in Fig. 9]. As is clear from Fig. 10, the singularity in the EDJDOS falls in fact in a region where $\partial f/\partial T$ is zero, reducing the resulting area.

On increasing the photon energy, the CEDS's will have part of their surface in region L (which experiences a *decrease* of electron population) so that the net change of absorption will start a rather fast decrease [arrow (e) in Fig. 9].

For $\hbar\omega = 3.901$ eV, CEDS VI, owing to its cur-

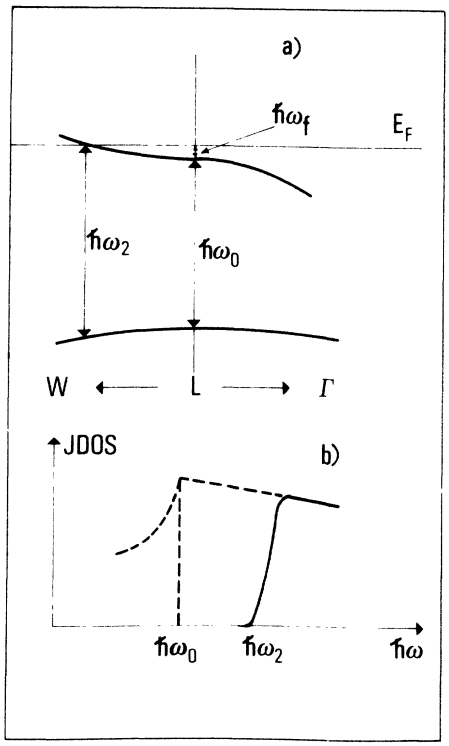

FIG. 11. (a) Bands responsible for $d \rightarrow p$ transition in Ag. (b) Schematic joint density of states for the $d \rightarrow p$ transition in Ag (solid line).

vature, has a larger part of its surface in region L than in region U. Besides, the singularity in the EDJDOS falls in the region where $\partial f/\partial T$ is negative and this results in a strong contribution of the negative area. For even higher photon energies, the change in absorption goes to zero, because the CEDS's have roughly equal areas in regions U and L. The singularity in the EDJDOS falls outside the region where $\partial f/\partial T$ is significantly different from zero so that the positive and negative lobes are weighted roughly equally.

This analysis clearly shows that the thermoderivative signal arises in noble metals from a very small and localized region of the Brillouin zone (in practice, the neck regions very close to the hexagonal faces).

It is also interesting to note that the cruder two-OPW (orthogonal plane wave) approximation often used to explain photoemission results[32,41] completely fails to explain the origin of thermomodulation signal. In this approximation, the CEDS's are planes perpendicular to Λ and the EDJDOS turns out to be a constant. The CEDS's have roughly equal portions of their surfaces in region U and region L, giving rise to a zero net change of absorption.

III. TRANSITIONS FROM d BANDS TO THE FERMI SURFACE

A. Static joint density of states

Referring to Fig. 2 it is clear that if the p band were completely empty, the $d \rightarrow p$ transitions would give an M_1-type critical point in the joint density of states. Since the band is filled for a few tenths of an eV above L_2', we can have optical transitions only for photon energies above a threshold $\hbar\omega_2$ [shown in Fig. 11(a)]. The shape of the JDOS which we expect is shown schematically in Fig. 11(b).

Assuming, also, the d-band energy depends quadratically on the distance from L, we may write

$$\hbar\omega_d \equiv -\hbar\omega_f - \hbar\omega_0 - \frac{\hbar^2}{2m_{d\perp}} k_\perp^2 - \frac{\hbar^2}{2m_{d\parallel}} k_\parallel^2 \ . \qquad (22)$$

We already know the constant-energy surfaces for the p band [Eq. (7)]. The constant-energy surfaces for the d band are easily obtained:

$$\hbar\omega_d \equiv -\hbar\omega_f - \hbar\omega_0 - \frac{\hbar^2}{2m_{d\perp}} k_\perp^2 - \frac{\hbar^2}{2m_{d\parallel}} k_\parallel^2 = E - \hbar\omega \ . \qquad (23)$$

The JDOS for the $d \rightarrow p$ transitions can be written as

$$\mathcal{J}_{d\rightarrow p}(\hbar\omega) = (2\pi)^{-3} \int' \frac{dS_{p\rightarrow d}}{|\nabla_{\vec{k}}(\hbar\omega_p) - \nabla_{\vec{k}}(\hbar\omega_d)|} \ , \qquad (24)$$

the integral being now carried out (for each photon energy) over the surface $\Omega_{pd}(k) = 0$. The CEDS can be obtained by subtracting Eq. (23) from Eq. (7):

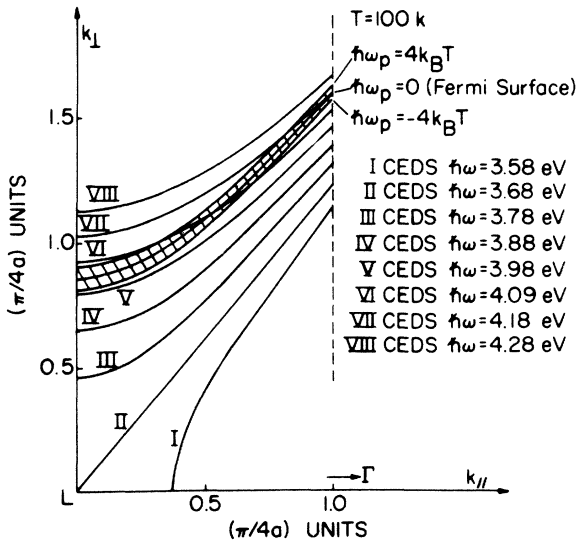

FIG. 12. Cross section in the Fermi-surface neck region of CEDS ($d \rightarrow p$ bands) in a plane containing the L-Γ direction. Also shown are the constant-initial-energy surfaces $E = -4k_BT$, $E = 0$ (Fermi surface), and $E = 4k_BT$.

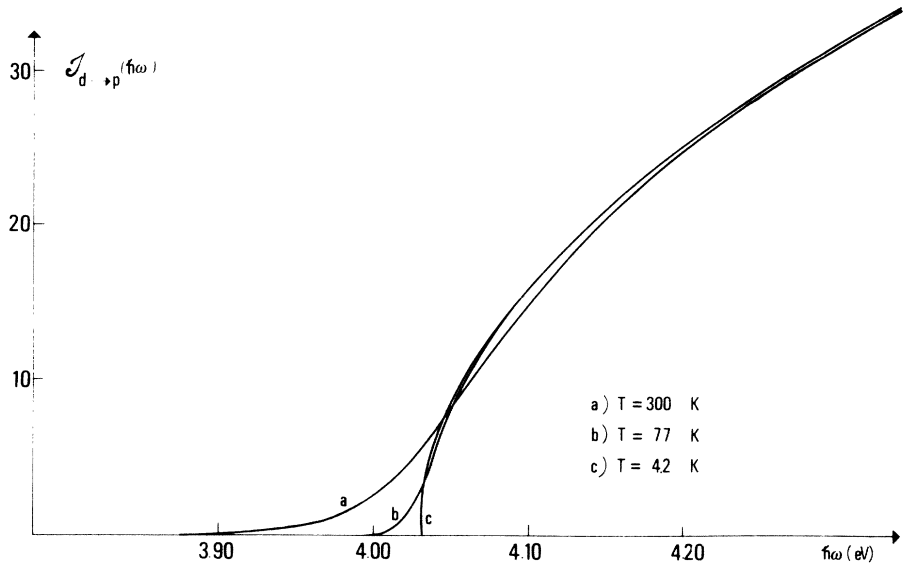

FIG. 13. Joint density of states (JDOS) of Ag due to the $d \rightarrow p$-band transitions near L calculated at different temperatures.

$$\Omega_{pd}(\vec{k}) \equiv \hbar\omega_0 + \frac{\hbar^2}{2}\left(\frac{1}{m_{p\perp}} + \frac{1}{m_{d\perp}}\right)k_\perp^2 + \frac{\hbar^2}{2}\left(\frac{1}{m_{d\parallel}} - \frac{1}{m_{p\parallel}}\right)k_\parallel^2 - \hbar\omega = 0. \quad (25)$$

Figure 12 gives some (110) sections of these CEDS's together with the (110) section of the Fermi surface. It can be noticed that the CEDS's now run almost parallel to the Fermi surface. This is, of course, due to the flatness of the d band: We can expect therefore a much sharper onset of the JDOS than in the preceding case.

There is another important difference from the case of the $p \rightarrow s$ transitions: On increasing the photon energy, the CEDS's now tend to run out of the Fermi surface. Since the points inside the Fermi surface represent occupied states in the p bands, only the regions of each CEDS exposed

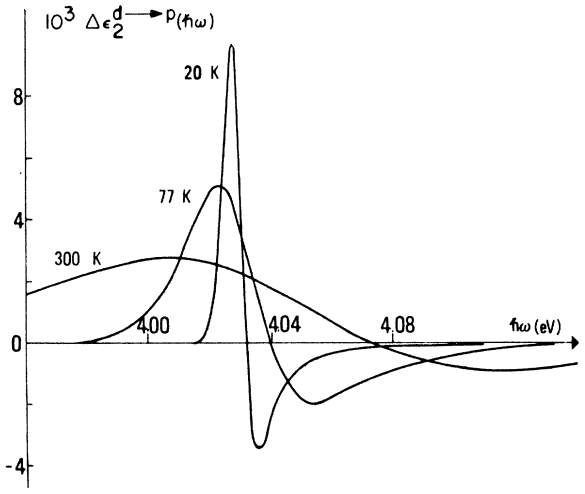

FIG. 14. $\Delta\epsilon_2$ thermomodulation spectra calculated at different temperatures arising from $d \rightarrow p$-band transitions in Ag.

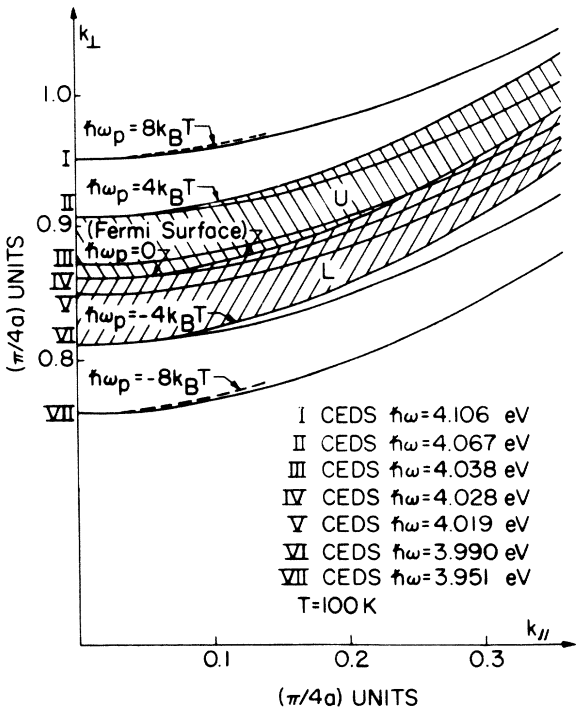

FIG. 15. Detail of the Fermi-surface neck region showing several (110) cross sections of CEDS's ($d \rightarrow p$ bands) and constant-final-energy surfaces.

above the Fermi surface can contribute to the absorption.

In calculating the JDOS $(\hbar\omega, T)$, again, each infinitesimal ribbon of a CEDS, corresponding to transitions with final energy between E and $E+dE$, has to be weighted with the probability that the final state is empty $[1-f(E)]$. For this calculation we resort again to the energy distribution of the joint density of states:

$$\mathfrak{D}_{d\to p}(E,\hbar\omega) = (2\pi)^{-3}\int \frac{dl_{pd}}{|\nabla_{\vec{k}}(\hbar\omega_p)\times\nabla_{\vec{k}}(\hbar\omega_d)|} \quad . \tag{26}$$

The integral is performed around the line of intersection of the two constant-energy surfaces $\hbar\omega_p = E$ and $\hbar\omega_d = E-\hbar\omega$. The latter are now ellipsoids with centers at L and rotational symmetry around the Γ-L direction. The paths of integration therefore are again circles on planes perpendicular to Λ and are centered on the Λ axis.

Inserting Eqs. (1) and (22) into Eq. (26), we obtain

$$\mathfrak{D}_{d\to p}(E,\hbar\omega) = (16\pi^2\hbar^2)^{-1}\mathfrak{F}_{d\to p} \times\left(\frac{\hbar}{m_{p\perp}}(\hbar\omega-\hbar\omega_0-\hbar\omega_f-E) - \frac{\hbar}{m_{d\perp}}(E+\hbar\omega_f)\right)^{-1/2} , \tag{27}$$

where the geometric factor $\mathfrak{F}_{d\to p}$ is given by

$$\mathfrak{F}_{d\to p} = \left(\frac{m_{d\parallel}}{m_{d\parallel}}\frac{m_{p\perp}+m_{d\perp}}{m_{p\perp}}\frac{m_{p\parallel}}{m_{d\perp}\,m_{p\parallel}}\right)^{-1/2} . \tag{28}$$

The joint density of states is given by

$$\mathfrak{J}_{d\to p}(\hbar\omega, T) = \int_{E_{min}}^{E_{max}} \mathfrak{D}_{d\to p}(E,\hbar\omega)\,[1-f(E,T)]\,dE \quad . \tag{29}$$

Straightforward algebra gives for the upper limit of integration

$$E_{max} = -\hbar\omega_f + \frac{m_{d\parallel}}{m_{d\parallel}-m_{p\parallel}}(\hbar\omega-\hbar\omega_0) \quad \text{for } \hbar\omega<\hbar\omega_0 \tag{30}$$

and

$$E_{max} = -\hbar\omega_f + \frac{m_{d\perp}}{m_{p\perp}+m_{d\perp}}(\hbar\omega-\hbar\omega_0) \quad \text{for } \hbar\omega>\hbar\omega_0 \quad . \tag{31}$$

The lower limit of integration has been chosen at the intersection of each CEDS with the plane perpendicular to Λ at a distance $\pi/4a$ from L. We obtain

$$E_{min} = -\hbar\omega_f - \frac{\hbar^2}{2m_{p\parallel}}\left(\frac{\pi}{4a}\right)^2 + \frac{m_{p\perp}}{m_{p\perp}+m_{d\perp}} \times\left[\frac{\hbar}{2}\left(\frac{1}{m_{p\parallel}}-\frac{1}{m_{d\parallel}}\right)\left(\frac{\pi}{4a}\right)^2+(\hbar\omega-\hbar\omega_0)\right] \quad . \tag{32}$$

Figure 13 shows $\mathfrak{J}_{d\to p}(\hbar\omega)$ for three different temperatures. The magnitude is determined partly by the geometrical factor given by Eq. (28) and partly by the matrix element of the transitions. This latter has been again determined by comparison with the experimental structures (see paper II).

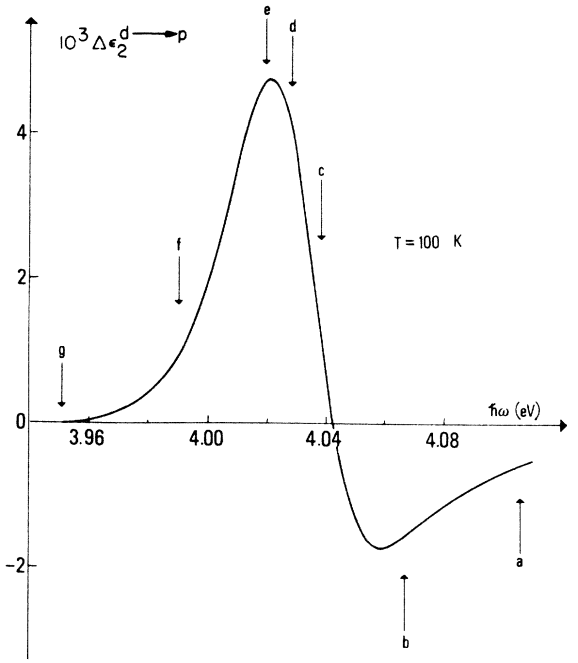

FIG. 16. $\Delta\epsilon_2$ thermomodulation spectrum for $d\to p$ transitions in Ag at 100 K. Arrows (a)–(g) indicate the situation corresponding to the CEDS's I–VII, respectively, shown in Fig. 15.

B. Thermoderivative behavior

Differentiating Eq. (29) and using Eq. (15), we obtain

$$\Delta\epsilon_2^{d\to p}(\hbar\omega, T) = \frac{8\pi^2e^2\hbar^4}{3m^2}\frac{|P(d\to p)|^2}{(\hbar\omega)^2}\frac{\partial}{\partial T}(\mathfrak{J}_{d\to p}(\hbar\omega, T))\,\Delta T, \tag{33}$$

where

$$\frac{\partial}{\partial T}(\mathfrak{J}_{d\to p}(\hbar\omega, T)) = \int_{E_{min}}^{E_{max}} \mathfrak{D}_{d\to p}(E,\hbar\omega)\left(-\frac{\partial f(E,T)}{\partial T}\right)dE . \tag{34}$$

Figure 14 shows the spectra of $\Delta\epsilon_2^{d\to p}$ calculated at different temperatures, again assuming $\Delta T = 1$ K. Lowering the temperature we have again a sharpening of the structures as well as an enhancement. However, by comparing spectra obtained at the same temperature in Figs. 8 and 14, one sees that the $d\to p$ transitions give broader structures. The reason for this can be seen easily by differentiating Eqs. (16) and (31):

$$\frac{\Delta E}{\Delta(\hbar\omega)} = -\frac{m_{s\perp}}{m_{s\perp}-m_{p\perp}} = -1.07 \quad (p\to s) \tag{35}$$

and

$$\frac{\Delta E}{\Delta(\hbar\omega)} = \frac{m_{d\perp}}{m_{d\perp} + m_{p\perp}} = 0.89 \quad (d \rightarrow p) \ , \tag{36}$$

which show that the CEDS's rate of spanning the region where a modulation signal is produced is larger for the $p \rightarrow s$ transitions than for the $d \rightarrow p$ transitions. The former therefore tend to yield larger signals.

In order to follow the mechanism of modulation in this case, Fig. 15 shows the (110) section of the Fermi surface in the neck region together with sections of some CEDS's, starting, respectively, $-8k_BT$, $-4k_BT$, $-k_BT$, 0, $+k_BT$, $+4k_BT$, and $+8k_BT$ away from the neck (with $T = 100$ K). Figure 16 gives a detailed plot of $\Delta\epsilon_2^{d\rightarrow p}$ for $T = 100$ K. The arrows show the situation corresponding to each of the CEDS's shown in Fig. 15.

IV. CONCLUSIONS

A very simple model has been set up which allows the calculation of the static and thermoderivative behavior (in the low-temperature limit) of the dielectric function for optical transitions in noble metals involving the Fermi surface. The results obtained for Ag can be extended easily to Cu and Au.

[1]H. Ehrenreich and H. R. Philipp, Phys. Rev. 128, 1622 (1962).
[2]B. R. Cooper, H. Ehrenreich, and H. R. Philipp, Phys. Rev. 138, A494 (1965).
[3]B. Segall, Phys. Rev. 125, 109 (1962).
[4]G. A. Burdick, Phys. Rev. 129, 138 (1963).
[5]D. Beaglehole, Proc. Phys. Soc. Lond. 85, 1007 (1965); 87, 461 (1966).
[6]F. M. Mueller and J. C. Phillips, Phys. Rev. 157, 600 (1967).
[7]G. Dresselhaus, Solid State Commun. 7, 419 (1969).
[8]A. R. Williams, J. F. Janak, and V. L. Moruzzi, Phys. Rev. Lett. 28, 671 (1972).
[9]N. E. Christensen and B. O. Seraphin, Phys. Rev. B 4, 3321 (1971).
[10]N. E. Christensen, Phys. Status Solidi B 54, 551 (1972).
[11]C. N. Berglund and W. E. Spicer, Phys. Rev. 136, A1044 (1964).
[12]W. E. Spicer, Phys. Rev. 154, 385 (1967).
[13]W. F. Krolikowski and W. E. Spicer, Phys. Rev. 185, 882 (1969).
[14]N. V. Smith, Phys. Rev. Lett. 23, 1452 (1969).
[15]D. E. Eastman and J. K. Cashion, Phys. Rev. Lett. 24, 310 (1969).
[16]P. O. Nilsson, C. Norris, and L. Walldén, Phys. Kondens. Mater. 11, 220 (1970).
[17]I. Lindau and L. Walldén, Phys. Scr. 3, 77 (1971).
[18]G. P. Pells and M. Shiga, J. Phys. C 2, 1835 (1969).
[19]R. M. Morgan and D. W. Lynch, Phys. Rev. 172, 628 (1968).
[20]E. L. Green and L. Muldawer, Phys. Rev. B 2, 330 (1970).
[21]M. L. Thèye, Phys. Rev. B 2, 3060 (1970).
[22]M. Welkowsky and R. Braunstein, Solid State Commun. 9, 2139 (1971).
[23]H. G. Liljenvall and A. G. Mathewson, J. Phys. C Suppl. Met. Phys. 3, 341 (1970).
[24]P. B. Johnson and R. W. Christy, Phys. Rev. B 6, 4370 (1972).
[25]M. Garfinkel, J. J. Tiemann, and W. E. Engeler, Phys. Rev. 148, 695 (1966).
[26]U. Gerhardt, Phys. Rev. 172, 651 (1968).
[27]C. E. Morris and D. W. Lynch, Phys. Rev. 182, 719 (1969).
[28]W. J. Scouler, Phys. Rev. Lett. 18, 455 (1967).
[29]P. O. Nilsson and B. Sandell, Solid State Commun. 8, 721 (1970).
[30]B. F. Schmidt and D. W. Lynch, Phys. Rev. B 3, 4015 (1971).
[31]N. V. Smith, Phys. Rev. B 3, 1862 (1971).
[32]L. Walldén and T. Gustafsson, Phys. Scr. 6, 73 (1972).
[33]N. E. Christensen, in *Proceedings of the International Symposium on Computational Physics*, edited by F. Herman, N. W. Dalton, and T. R. Koehler (Plenum, New York, 1972), p. 155.
[34]Recent investigations give for the $L_2' \rightarrow L_1$ critical point the values 4.15 (Ref. 27), 4.25 (Ref. 30), 4.17 (Ref. 32), and 3.49 eV (Ref. 10).
[35]R. Rosei, F. Antonangeli, and U. M. Grassano, Surf. Sci. 37, 689 (1973).
[36]R. Rosei, C. H. Culp, and J. H. Weaver, following paper, Phys. Rev. B 10, 484 (1974).
[37]The zero of energy and wave number are defined at E_F and L, respectively.
[38]G. F. Bassani, *Rendiconti della Scuola Internazionale di Fisica E. Fermi, XXXIV Corso, Varenna*, 1965 (Academic, New York, 1966), p. 33.
[39]J. C. Phillips, Solid State Phys. 18, 55 (1966).
[40]The numerical values of the effective masses have been calculated by fitting parabolas to the bands given in Ref. 10 (with the exception of $m_{p\perp}$, which has been taken from Ref. 32) and adjusting the energy gaps in order to give good agreement with the experimental results presented in paper II.
[41]R. Y. Koyama and N. V. Smith, Phys. Rev. B 2, 3049 (1970).
[42]D. Brust, Phys. Rev. 139, A489 (1965).
[43]E. O. Kane [in Phys. Rev. 175, 1039 (1968)] in his theory of critical points in photoelectric emission energy distributions finds a logarithmic singularity for the saddle-point case. In the present case, however, owing to the circular symmetry assumed around the Γ-L direction a CEDS becomes tangent to a constant-energy surface not only in an isolated point but along a whole line, so that is topologically different.
[44]See, for instance, Ref. 31.
[45]R. Rosei and D. W. Lynch, Phys. Rev. B 5, 3883 (1972).